Statistical Downscaling of IPCC Sea Surface Wind and Wind Energy Predictions for U.S. East Coastal Ocean, Gulf of Mexico and Caribbean Sea

YAO Zhigang[1), 2), *], XUE Zuo[2), 3)], HE Ruoying[2)], BAO Xianwen[1)], and SONG Jun[4)]

1) *Key Laboratory of Physical Oceanography, Ocean University of China, Qingdao* 266071, *P. R. China*
2) *Department of Marine, Earth and Atmospheric Sciences, North Carolina State University, Raleigh, NC* 27695, *USA*
3) *Department of Oceanography and Coastal Sciences, Louisiana State University, Baton Rouge* 70803, *USA*
4) *National Marine Data and Information Service, Tianjin* 300171, *P. R. China*

Abstract A multivariate statistical downscaling method is developed to produce regional, high-resolution, coastal surface wind fields based on the IPCC global model predictions for the U.S. east coastal ocean, the Gulf of Mexico (GOM), and the Caribbean Sea. The statistical relationship is built upon linear regressions between the empirical orthogonal function (EOF) spaces of a cross-calibrated, multi-platform, multi-instrument ocean surface wind velocity dataset (predictand) and the global NCEP wind reanalysis (predictor) over a 10 year period from 2000 to 2009. The statistical relationship is validated before applications and its effectiveness is confirmed by the good agreement between downscaled wind fields based on the NCEP reanalysis and *in-situ* surface wind measured at 16 National Data Buoy Center (NDBC) buoys in the U.S. east coastal ocean and the GOM during 1992–1999. The predictand-predictor relationship is applied to IPCC GFDL model output (2.0°×2.5°) of downscaled coastal wind at 0.25°×0.25° resolution. The temporal and spatial variability of future predicted wind speeds and wind energy potential over the study region are further quantified. It is shown that wind speed and power would significantly be reduced in the high CO_2 climate scenario offshore of the mid-Atlantic and northeast U.S., with the speed falling to one quarter of its original value.

Key words climate changes; statistical downscaling; surface winds

1 Introduction

Coupled (atmosphere-ocean) Global Circulation Models (CGCMs) are important tools to project climate variability under different greenhouse gas emission scenarios. However, their abilities to resolve the regional/local climate changes are largely compromised by coarse resolutions, which typically range from 125 to 400 km for CGGMs participating in IPCC (Intergovernmental Panel on Climate Change) model assessment (Bracegirdle *et al.*, 2013; IPCC, 2007a). Regional downscaling is much needed to project coarse-resolution climate model solutions to finer regional resolutions, so that detailed local climate projections can be derived. This is especially relevant for coastal regions, which are vulnerable to threats including changes in strengths and patterns of coastal storms and sea level rise associated with glacial melting and thermal expansion of ocean waters.

Regional downscaling methods can be categorized into either dynamical or statistical approach. Dynamical down-

scaling uses nested high-resolution models, which are very costly to implement. Statistical downscaling offers a much more cost-effective means, as demonstrated by recent studies of land surface wind (Najac *et al.*, 2009; Pryor *et al.*, 2006; Sailor *et al.*, 2000; Salameh *et al.*, 2009) and the variability of surface wind over the Atlantic Ocean (Cassou *et al.*, 2011) and other surface atmospheric variables (Gutiérrez *et al.*, 2012; Dayon *et al.*, 2015; Minvielle *et al.*, 2011). In this study we took a multivariate, high-resolution, statistical downscaling approach to analyze regional coastal surface wind fields for the U.S. east coastal ocean, the Gulf of Mexico and the Caribbean Sea.

2 Methods and Data

Fundamentals to the statistical downscaling method used in this study are the building of a statistical relationship between local/regional variables (predictands) and large-scale climate characteristics (predictors) for the present day climate. This relationship is subsequently applied to the large-scale CGCM's outputs for different climate scenarios of interest for the future. Here we adopted a statistical downscaling approach introduced by Goubanova *et al.* (2011), which generated sea-surface

wind in the Peru-Chile upwelling region based on IPSL-CM4 model output. Specifically, the statistical model applied a multiple linear regression between the 'predictand', a cross-calibrated, multi-platform (CCMP), multi-instrument ocean surface wind velocity dataset (http://sivo.gsfc.nasa.gov/oceanwinds), and the 'predictor', which included the large-scale meridional wind, zonal wind, and sea level pressure (SLP) data produced by NOAA NCEP (National Centers for Environmental Prediction) reanalysis for the same CCMP data period. The NCEP reanalysis data have comparable spatial resolution to that of the IPCC's CGCMs.

The predictor-predictant relationship was built in the empirical orthogonal functions (EOF) space. For the predictant (daily, 0.25°×0.25° resolution, CCMP zonal and meridional wind fields), the EOFs were obtained based on the anomalies relative to the mean seasonal cycle for the period 1999–2009. We retained the first 15 EOFs, which explain more than 80% of the total variance. For the predictor (daily, 2.5°×2.5° resolution NCEP SLP, zonal and meridional wind fields), the EOFs were computed in the same fashion for the same time period. We found that the first 20 EOFs of the predictor must be included in order to explain more than 80% of the total variance (Table 1).

Table 1 Statistics of the ten predictand PCs used in the downscaling

	PC1	PC2	PC3	PC4	PC5	PC6	PC7	PC8	PC9	PC10
EV (NCEP)	32.84	17.61	10.71	7.01	5.03	3.84	3.02	2.24	1.79	1.38
EV (CCMP)	25.67	22.39	8.46	7.46	5.07	4.56	3.39	2.57	1.98	1.85
SD	424.54	396.48	243.66	228.86	188.69	178.93	154.22	134.35	117.78	113.84
SE	50.47	42.75	51.36	36.70	39.98	38.96	38.24	37.12	37.94	55.07
SE/SD	0.12	0.11	0.21	0.16	0.21	0.22	0.25	0.28	0.32	0.48

Notes: EV, Percentage of total variance explained by each PC; SD, Standard deviation for each PC; SE, Standard deviation of regression error ε.

The predictor-predictant relationship was then built in the principal components corresponding to the retained EOFs based on the following formulation:

$$PC\_Q_i = \sum_{j=1}^{20} \alpha_{i,j} \times PC\_N_j + \varepsilon, \ i=1{:}15, \qquad (1)$$

where PC_Q_i is the ith CCMP Principal Component (PC) time series, PC_N_j are the PCs of the NCEP reanalysis, $\alpha_{i,j}$ are the regression coefficients determined by the least square fitting method, and ε is the regression error.

To downscale the CGCM solutions (2.0°×2.5° resolution Geophysical Fluid Dynamics Laboratory CM2.1) for two different climate scenarios, we first computed the anomalies of the corresponding predictor variables (GFDL CM2.1 simulated meridional wind, zonal wind, and SLP) relative to their mean seasonal cycles, which were derived from the GFDL CM2.1 (20C3M run) for the period 1970–1999. Taking X as the anomalies of predictors for a given climate scenario, we then projected X onto EOF_N_j space derived in (1) to obtain the corresponding PCs and applied the same set of regression coefficients derived in (1) to these projections. The resulting PC_X time series associated with a given climate scenario can be derived over a coastal region of interest at higher resolution:

$$PC\_X_i = \sum_{j=1}^{20} \alpha_{i,j} \times (X \cdot EOF\_N_j), \ i=1{:}15. \qquad (2)$$

Finally, the downscaled fields were constructed following:

$$Y_{DS} = PC\_X \cdot EOF\_Q, \qquad (3)$$

where EOF_Q are the 0.25°×0.25° resolution CCMP ei-

genfunctions, and Y_{DS} are the downscaled anomalies of 0.25°×0.25° resolution meridional and zonal wind field anomalies. The total wind fields can be obtained by adding the anomalies with present-day seasonal cycle derived from CCMP.

3 Statistical Model Validation

In order to validate the statistical model expressed in Eqs. (1) to (3), we compared our downscaled wind fields (at 0.25°×0.25° resolution) based on NCEP reanalysis against *in-situ* surface wind measured at 16 National Data Buoy Center (NDBC) buoys in the U.S. east coastal ocean and the Gulf of Mexico (GOM) during 1992–1999. Fig.1, for example, indicates a good agreement between year-long time series of observed and downscaled wind at three buoys: one in the Middle Atlantic Bight (MAB), one in the South Atlantic Bight (SAB), and the other in the GOM.

Table 2 summarizes comparisons at all 16 stations using correlation coefficients (R) and root mean square errors (RMSE) between the observed and downscaled winds. Both forms of the comparisons (*i.e.*, the correlation coefficients at most of stations are greater than 0.6) suggest that the statistical downscaling model works well in capturing the temporal and spatial variability in both meridional and zonal winds. The downscaled model performed best in the winter season (when winds are typically stronger) and resembled better the observed winds at open-ocean stations (*e.g.*, stations 41001, 41004, and 44025) than at coastal stations (*e.g.*, stations SRST2 and 42035), suggesting that more refined wind downscaling would be needed to better resolve complex near-shore topographic/orographic features that may affect the model's accuracy.
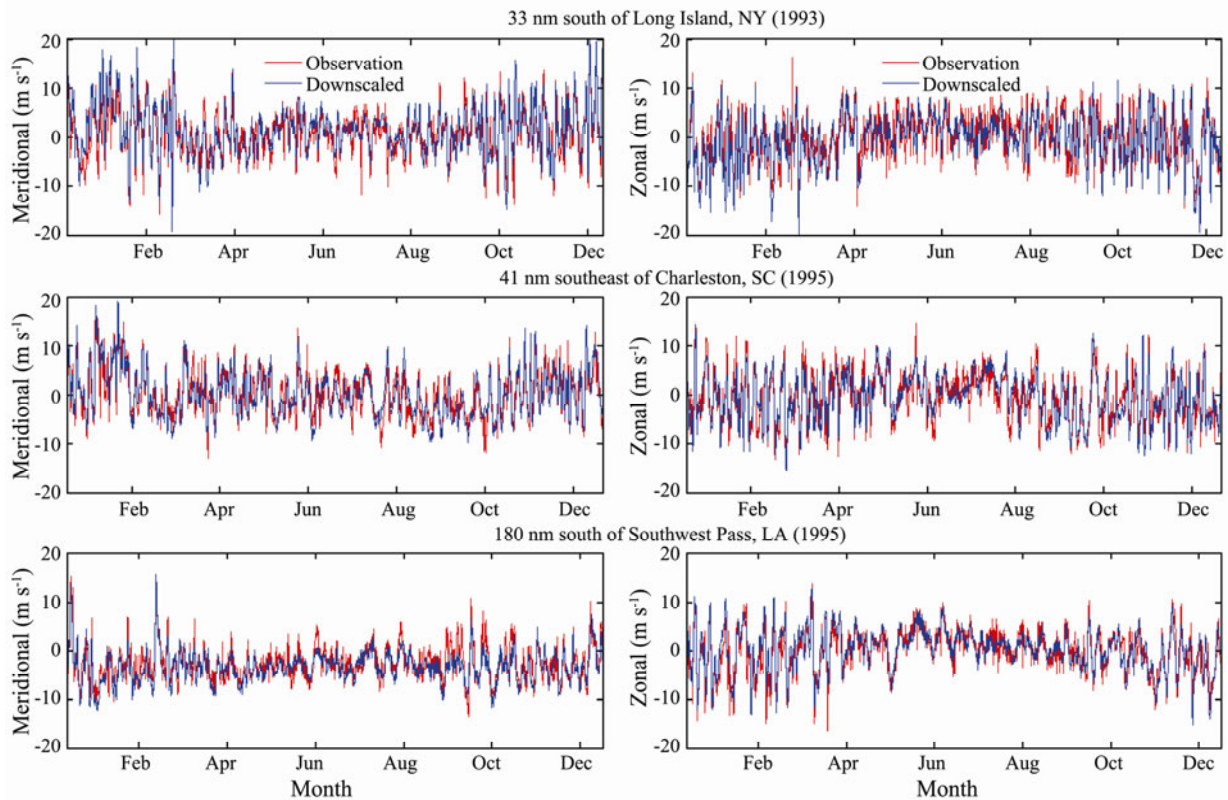
Fig.1 Comparisons between observed and downscaled wind (meridional and zonal wind speeds) at three NDBC buoys in the U.S. east coastal ocean and the Gulf of Mexico. Comparisons were done for the period 1992–1999 and summarized in Table 1. Here only three year-long time series comparisons are shown as an example.

Table 2 Correlation coefficients and root mean square errors (RMSE) between observed and downscaled winds at 16 NDBC buoys in the U.S. east coastal ocean and the Gulf of Mexico from 1992–1999

Station ID	Location	Lon	Lat	# of Obs.	R		RMSE	
					u	v	u	v
44007	12 nm southeast of Portland, ME	−70.144	43.531	8449	0.74	0.64	2.55	3.60
44005	78 nm east of Portsmouth, NH	−69.140	43.189	7507	0.81	0.80	3.00	3.29
44013	16 nw east of Boston, MA	−70.651	42.346	9230	0.78	0.70	3.02	3.35
BUZM3	Buzzards Bay, MA	−71.033	41.397	5296	0.81	0.75	3.14	3.85
44025	33 nm south of Long Island, NY	−73.166	40.250	10097	0.80	0.74	3.17	3.38
44009	26 nw southeast of Cape May, NJ	−74.702	38.464	8649	0.76	0.76	2.88	3.48
CHLV2	Chesapeake Light, VA	−75.710	36.910	9997	0.74	0.77	3.08	3.89
41001	150 nw east of Cape Hatteras, NC	−72.698	34.675	7547	0.82	0.84	3.16	3.24
CLKN7	Cape Lookout, NC	−76.525	34.622	10169	0.76	0.78	2.94	3.30
41004	41 nw southeast of Charleston, SC	−79.099	32.501	6273	0.82	0.78	2.83	3.18
LKWF1	Lake Worth, FL	−80.033	26.612	6963	0.72	0.73	2.71	2.71
KTNF1	Keaton Beach, FL	−83.592	29.817	5189	0.68	0.59	2.6	2.57
BURL1	Southwest Pass, LA	−89.428	28.905	9874	0.73	0.77	2.94	3.06
42001	180 nw south of Southwest Pass, LA	−89.667	25.900	9713	0.78	0.80	2.45	2.75
SRST2	Sabine Pass, TX	−94.033	29.683	9693	0.63	0.70	2.45	3.10
42035	Galveston, TX	−94.413	29.232	6571	0.67	0.77	2.63	3.04

Notes: R, correlation coefficient; RMSE, root mean square standard error, unit: m s^{-1}.

4 Applications to Different Climate Scenarios

The GFDL CM2.1 climate model predictions of surface wind fields were statistically downscaled using the same method above. The method is extremely efficient compared with the dynamical downscaling approach. The simulation to produce a 100 year (2001–2100) statistical wind downscaling only took about 1 hour to complete on a single processor Linux computer. We chose two climate emission scenarios: the pre-industrial (PI) scenario and

the A1F1 scenario. The higher-emission A1F1 scenario represents a future condition in which fossil fuel-intensive, rapid economic growth occurs, and a global population peaks in the mid-century and then declines afterward. In this scenario, concentrations of atmospheric carbon dioxide reach 940 ppm by 2100, which is more than triple Pre-Industrial level (which is about 280 ppm in the PI scenario) (IPCC, 2007b, 2013).

Fig.2 shows the downscaled wind fields in the IPCC PI and A1F1 emission scenarios averaged for April in 2069–2079. We present these results because: 1) the IPCC projected concentration of atmospheric carbon dioxide reaches a relatively steady rate of increase after 2060; 2) their April means clearly demonstrate the wind responses to different climate change scenarios.

In both PI and A1F1 scenarios, the April mean surface winds are stronger in the southwest Caribbean than in other areas. There, the maximum wind speed is 9.6 m s^{-1} and 10.0 m s^{-1} in the PI scenario and the A1F1 scenario,

respectively. Surface wind speeds are reduced in the MAB with the maximum wind speed being 8.9 m s^{-1} and 7.2 m s^{-1} in the PI scenario and the A1F1 scenario, respectively. Winds in the SAB and GOM are relatively weaker in both scenarios. The difference in wind speed between the two scenarios (Fig.2c; A1F1 wind speed minus PI wind speed) shows that there is an overall decrease in the mean wind speed from the PI to the A1F1 scenario. The spatially averaged difference is 0.15 m s^{-1}. The most significant decreases are seen offshore of the U.S. east coast, and along the west coast of Florida. There the maximum wind speeds in the A1F1 scenario are reduced by up to 26% in the north Atlantic and 24% in the Gulf of Mexico compared with the PI scenario. A small increase in wind speed is found in the southern Gulf of Mexico and the Caribbean Sea. A similar spatial pattern has also been reported by Wang *et al.* (2014) for significant wave height changes based on the analysis of 20 CMIP5 climate model results.
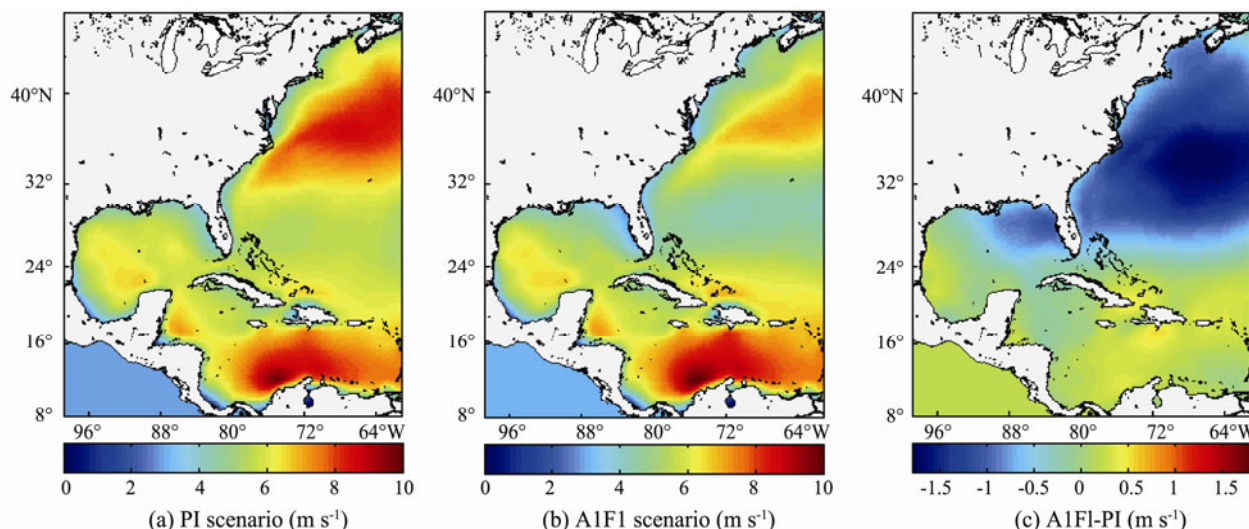

Fig.2 Downscaled April mean wind speed fields in (a) the Pre-Industrial scenario and (b) the A1F1 scenario (c) Wind field difference between the scenarios (A1F1 minus Pre-Industrial).
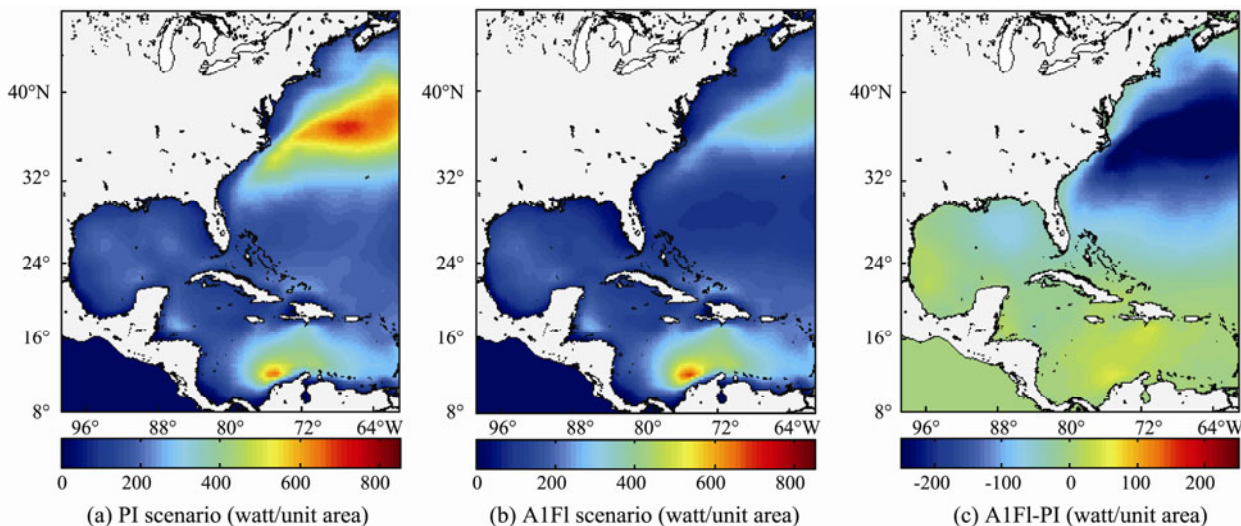

Fig.3 Calculated April mean wind energy in (a) Pre-Industrial scenario, (b) A1F1 scenario, (c) Wind power difference between the two scenarios (A1F1 minus Pre-Industrial).

Given that wind is a promising source of renewable energy, we can use the resulting downscaled regional wind projections to further explore wind energy as a resource in the two climate scenarios. Wind energy potential is proportional to the wind speed cubed and can be computed as:

$$P = 0.5 \cdot rho \cdot V^3, \qquad (4)$$

where P is the power (watts per unit area), rho is the air density (taken as $1.225 \, \text{kg} \, \text{m}^{-3}$ at sea level), and V is the wind speed ($\text{m} \, \text{s}^{-1}$).

Using the long-term (2069–2079) April monthly average in PI and A1F1 scenarios, we see that the corresponding wind energy potentials have patterns similar to their wind fields (Fig.3). Higher wind energy potentials are projected offshore of the MAB and in the southwest Caribbean in both PI and A1F1 scenarios (Figs.3a and 3b). Specifically offshore of the mid-Atlantic, the energy maxima for the PI (A1F1) scenario can be found with a value of 698.1 (385.6) watts per unit area. The difference between the two scenarios (Fig.3c) shows the wind energy potential would decrease in high-CO_2 A1F1 offshore of the mid-Atlantic and northeast U.S., where a maximum decrease of 322 watts per unit area is seen. Our results suggest that the power potential of wind energy could be protected by reducing global CO_2 emissions. In a feedback loop, the more wind energy we invest in now to replace fossil fuels (which increase CO_2), the more we will protect future potential wind energy production, because less CO_2 leads to less loss of wind speed.

5 Summary

We developed a highly efficient multivariate statistical method to assess the impact of climate change on regional wind fields for the U.S. east coast, the Gulf of Mexico and Caribbean Sea. The NASA cross-calibrated, multi-platform (CCMP), multi-instrument ocean surface wind velocity dataset and NOAA NCEP reanalysis were used to derive the statistical model, which was subsequently used to downscale IPCC GFDL climate model wind projections in Pre-Industrial and A1F1high-CO_2 A1F1 future scenarios. The downscaling allows refining of the representation of daily coastal winds and wind energy potential to a local scale. The model predicts that the average wind in April will significantly weaken in the A1F1 scenario relative to the PI scenario, especially offshore of the mid-Atlantic and northeast U.S., with the speed reduction reaching up to one quarter of its original value. Because the wind energy potential is proportional to the wind speed cubed, the wind weakening would also indicate a more than 50% reduction in wind power in those areas.

An additional application of the resulting downscaled wind fields is to use them to drive high-resolution coastal circulation models and to quantify storm-induced sea level variability in different climate scenarios. We will report findings of that study in a future correspondence. It should be mentioned that our wind downscale analysis may be limited by several factors/processes that were omitted in the method, such as air-sea couplings (Zambon *et al.*, 2014; Chelton *et al.*, 2004; Nelson *et al.*, 2014) and land-sea thermal contrast (Zhou and Zou, 2010), due to the limitations/biases of global CGCMs. Future research focusing on improving their representations in the downscaling analysis is still needed.

References

Bracegirdle, T. J., Shuckburgh, E., Sallee, J., Wang, Z., Meijers, A. J. S., Bruneau, N., Phillips, T., and Wilcox, L. J., 2013. Assessment of surface winds over the Atlantic, Indian, and Pacific Ocean sectors of the Southern Ocean in CMIP5 models: Historical bias, forcing response, and state dependence. *Journal of Geophysical Research: Atmospheres*, **118** (2): 547-562.

Cassou, C., Minvielle, M., Terray, L., and Périgaud, C., 2011. A statistical-dynamical scheme for reconstructing ocean forcing in the Atlantic. Part I: Weather regimes as predictors for ocean surface variables. *Climate Dynamics*, **36** (1-2): 19-39.

Chelton, D. B., Schlax, M. G., Freilich, M. H., and Milliff, R. F., 2004. Satellite measurements reveal persistent small-scale features in ocean winds. *Science*, **303** (5660): 978-983.

Dayon, G., Boé, J., and Martin, E., 2015. Transferability in the future climate of a statistical downscaling method for precipitation in France. *Journal of Geophysical Research: Atmospheres*, **120** (3): 2014J-22236J.

Goubanova, K., Echevin, V., Dewitte, B., Codron, F., Takahashi, K., Terray, P., and Vrac, M., 2011. Statistical downscaling of sea-surface wind over the Peru-Chile upwelling region: Diagnosing the impact of climate change from the IPSL-CM4 model. *Climate Dynamics*, **36** (7-8): 1365-1378.

Gutiérrez, J. M., San-Martín, D., Brands, S., Manzanas, R., and Herrera, S., 2012. Reassessing statistical downscaling techniques for their robust application under climate change conditions. *Journal of Climate*, **26** (1): 171-188.

IPCC (Intergovernmental Panel on Climate Change), 2007a. *Climate Change 2007: The Physical Science Basis*. Contribution of Working Group I to the Fourth Assessment Report of IPCC, Cambridge University Press, 996pp.

IPCC (Intergovernmental Panel on Climate Change), 2007b. *Climate Change 2007: Synthesis Report*. Contribution of Working Groups I, II and III to the Fourth Assessment Report of IPCC, Geneva, Switzerland, 104pp.

IPCC (Intergovernmental Panel on Climate Change), 2013. *Cli-*

mate Change 2013: The Physical Science Basis. Contribution of Working Group I to the Fifth Assessment Report of IPCC, Cambridge University Press, 1535pp.

Minvielle, M., Cassou, C., Bourdallé-Badie, R., Terray, L., and Najac, J., 2011. A statistical-dynamical scheme for reconstructing ocean forcing in the Atlantic. Part II: Methodology, validation and application to high-resolution ocean models. *Climate Dynamics*, **36** (3-4): 401-417.

Najac, J., Boé, J., and Terray, L., 2009. A multi-model ensemble approach for assessment of climate change impact on surface winds in France. *Climate Dynamics*, **32** (5): 615-634.

Nelson, J., He, R., Warner, J., and Bane, J., 2014. Air-sea interactions during strong winter extratropical storms. *Ocean Dynamics*, **64** (9): 1233-1246.

Pryor, S. C., Schoof, J. T., and Barthelmie, R. J., 2006. Winds of change?: Projections of near-surface winds under climate change scenarios. *Geophysical Research Letters*, **33**: L11702, DOI: 10.1029/2006GL026000.

Sailor, D. J., Hu, T., Li, X., and Rosen, J. N., 2000. A neural network approach to local downscaling of GCM output for assessing wind power implications of climate change. *Renewable Energy*, **19** (3): 359- 378.

Salameh, T., Drobinski, P., Vrac, M., and Naveau, P., 2009. Statistical downscaling of near-surface wind over complex terrain in southern France. *Meteorology and Atmospheric Physics*, **103** (1): 253-265.

Wang, X. L., Feng, Y., and Swail, V. R., 2014. Changes in global ocean wave heights as projected using multimodel CMIP5 simulations. *Geophysical Research Letters*, **41** (3): 1026-1034.

Zambon, J. B., He, R., and Warner, J., 2014. Investigation of hurricane Ivan using the coupled ocean-atmosphere-wave-sediment transport (COAWST) model. *Ocean Dynamics*, **64** (11): 1535-1554.

Zhou, T., and Zou, L., 2010. Understanding the predictability of East Asian summer monsoon from the reproduction of land-sea thermal contrast change in AMIP-type simulation. *Journal of Climate*, **23** (22): 6009-6026.

(Edited by Xie Jun)